

The CDF Time of Flight Detector

S. Cabrera^a, J. Fernández^a, G. Gómez^a, J. Piedra^{a,1}, T. Rodrigo^a, A. Ruiz^a,
I. Vila^a, R. Vilar^a, C. Grozis^b, R. Kephart^b, R. Stanek^b, D.H. Kim^c,
M.S. Kim^c, Y. Oh^c, Y.K. Kim^d, G. Veramendi^d, K. Anikeev^e, G. Bauer^e,
I.K. Furic^e, A. Korn^e, I. Kravchenko^e, M. Mulhearn^e, Ch. Paus^e,
S. Pavlon^e, K. Sumorok^e, C. Chen^f, M. Jones^f, W. Kononenko^f, J. Kroll^f,
G.M. Mayers^f, F.M. Newcomer^f, R.G.C. Oldeman^f, D. Usynin^f, R. Van
Berg^f, G. Bellettini^g, C. Cerri^g, A. Menzione^g, F. Spinella^g, E. Vataga^g,
S. De Cecco^h, D. De Pedis^h, C. Dionisi^h, S. Giagu^h, A. De Girolamo^h,
M. Rescigno^h, L. Zanello^h, M. Ahnⁱ, B.J. Kimⁱ, S.B. Kimⁱ, I. Cho^j, J. Lee^j,
I. Yu^j, H. Kaneko^k, A. Kazama^k, S. Kim^k, K. Sato^k, F. Ukegawa^k

^aInstituto de Física de Cantabria (CSIC - Universidad de Cantabria), Spain

^bFermi National Accelerator Laboratory, USA

^cKyungpook National University, Korea

^dLawrence Berkeley National Laboratory, USA

^eMassachusetts Institute of Technology, USA

^fUniversity of Pennsylvania, USA

^gINFN, University of Pisa, Italy

^hINFN, University of Roma, Italy

ⁱSeoul National University, Korea

^jSungKyunKwan University, Korea

^kUniversity of Tsukuba, Japan

Abstract

A new Time of Flight (TOF) detector based on scintillator bars with fine-mesh photomultipliers at both ends has been in operation since 2001 in the CDF experiment. With a design resolution of 100 ps, the TOF can provide separation between K^\pm and π^\pm in $p\bar{p}$ collisions at the 2σ level for low momentum, which enhances b flavor tagging capabilities. Because of its very fast response, the TOF is an excellent triggering device, and it is used to trigger on highly ionizing particles, multiple minimum ionizing particles and cosmic rays. Particle

identification is achieved by comparing the time-of-flight of the particle measured by the TOF to the time expected for a given mass hypothesis. In order to obtain the resolution necessary for particle ID, optimal calibrations are critical. This paper describes the TOF detector, its calibration procedure, the achieved resolution, the long term operation performances and some of the first results from data analysis using this detector.

1 Introduction

After the successful Run I data taking period at the Fermilab Tevatron from 1992 to 1996, the CDF detector has undergone a major upgrade [1] for the so-called Run II of the Tevatron, which began in March 2001. A Time of Flight (TOF) detector has been added to improve the particle identification capability. The installation of the TOF detector was completed in August 2001 and its data has been included in the CDF readout since that time.

During Run I, particle identification in CDF was based on the ionization energy loss, dE/dx , measured in the central drift chamber. The dE/dx measurement provided one standard deviation separation between charged kaons and charged pions for momenta greater than $2 \text{ GeV}/c$. The current CDF drift chamber, the Central Outer Tracker (COT), maintains this dE/dx performance. The primary physics motivation for TOF is to enhance the particle identification capability to improve neutral B meson flavor determination at production. With an expected time-of-flight resolution of 100 ps , the TOF system will provide at least two standard deviation separation between K^\pm and π^\pm for momenta $p < 1.6 \text{ GeV}/c$, complementing the dE/dx measurement from COT.

Particle identification with TOF is performed by measuring the time of arrival of a particle at the scintillator with respect to the collision time, t_0 . The particle mass m can then be determined from the momentum p , the path length L , and the time-of-flight t :

$$m = \frac{p}{c} \sqrt{\frac{c^2 t^2}{L^2} - 1} \quad (1)$$

where p and L are measured by the tracking system.

2 CDF TOF design

2.1 Mechanics

The CDF Time of Flight detector [2, 3, 4] consists of 216 bars of Bicron BC-408 scintillator with dimensions $4 \times 4 \times 279 \text{ cm}$ located between the COT and the cryostat of the super-conducting solenoid at a mean radius of 140 cm . The pseudo-rapidity coverage of the system is roughly $|\eta| < 1$.

The bars of scintillator were wrapped first in white Tyvek and a layer of black Marvelguard. The bars were assembled in groups of three by interleaving them with thin metal strips attached via springs to interlocking aluminum PMT housings at the ends to form a relatively rigid structure.

2.2 Photomultiplier Tubes and assembly

A Hamamatsu R7761 19-stage fine-mesh photomultiplier tube (PMT) with a diameter of 3.81 cm , is attached to each end of every bar. These can operate in the 1.4 T magnetic field of the CDF solenoid with an average gain reduction factor of 500 from the nominal gain of 10^6 . The optical connection between the PMT and the scintillator is made using a compound parabolic concentrator (CPC), attached to the PMT using optical cement. A good interface between the CPC and the scintillator is achieved using a silicone optical coupling pad that is compressed between them using the force applied by a spring. The voltage divider base is constructed using surface mount components on a printed circuit board, soldered directly to the leads of the PMT. A preamplifier is attached via a connector on the base. A small printed circuit board serves as a light seal and brings HV for the base and low voltage for the preamplifier into the assembly and signals from the preamplifier out. This entire assembly is mounted inside a 3.81 cm diameter hole bored in an aluminum block with the same transverse dimensions as the scintillator. A spring forces the assembly against the scintillator, insuring a good connection at the silicon optical coupling pad interface.

2.3 Front End Electronics

Figure 1 shows the signal path for a single PMT channel [5]. The preamplifier receives a nearly differential input formed from the anode and last dynode stage of the PMT. Its differential output is transmitted on shielded twisted

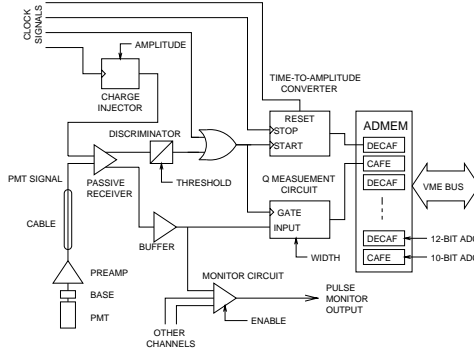


Figure 1: A block diagram of the electronics processing chain for the signal from one PMT channel. Most of the signals are indicated by single lines for clarity.

pair cable a distance of approximately 12 meters to the front-end electronics that resides in a VME crate mounted outside the detector. The received signal is split between two signal paths: one for the timing measurement and the other for a measurement related to the pulse height.

The timing path enters a discriminator whose output provides a start signal to a Time to Amplitude Converter (TAC). The TAC ramp is terminated by a common stop clock edge. The voltage output from the TAC is sampled by a 12-bit ADC. The common stop signal has its phase correctly adjusted with respect to the p and \bar{p} bunch crossing and is fanned out to all electronics channels in the system. This is implemented using a dedicated set of modules that first distributes differential ECL clock signals to each of 8 crates of electronics, and then to six TOF electronics modules within each crate. This same system generates a reset signal for the TAC and distributes it, along with a clock signal used for calibration, to all electronics channels.

The charge measurement path converts the received voltage signal from the preamplifier into a current that is passed to a charge sensitive ADC located on the ADC Memory Modules (ADMEMs). The current driver circuit is switched by a gate of adjustable width, initiated by the discriminator output, so that only the charge due to the pulse that fired the discriminator is integrated.

3 TOF Calibration

Without calibrating the response of each channel the timing resolution that can be achieved is of the order of a few nanoseconds. It is not possible to perform particle identification over any useful momentum range with a resolution this poor.

The operation of a Time of Flight detector in the CDF environment is unique in that it is not possible to synchronize a timing signal with respect to the $p\bar{p}$ interaction time. This is a consequence of the ~ 30 cm length of the p and \bar{p} bunches in the Tevatron which yields interactions spread out in time by a few nanoseconds. Not only does this complicate particle identification but it also makes it difficult to determine the parameters needed to calibrate individual channels.

3.1 Online Calibration

With such tight timing stability requirements, changes in the response of the electronics due to temperature variations, ground voltage shifts, or aging of the components are possible. The functionality for monitoring these effects is part of the electronics. Specifically, the time which corresponds to a particular value read out from the Time to Amplitude Converter (TAC) is determined periodically in the 'online' calibration runs taken during the time gap between consecutive Tevatron stores.

This calibration is performed using a digital delay generator DDG (Berkeley Nucleonics model B951) to initiate a differential ECL pulse that is fanned out to selected sets of channels. This signal is used to start the TAC, bypassing the discriminator. By stepping through a series of delays with respect to the common stop signal, the response of the TAC to known delays can be measured. Due to our demanding timing requirements we include a small non-linear correction to our TAC calibration, which is:

$$V_{TAC} = \beta(1 + \gamma e^{-t/\tau})t \quad (2)$$

where β , γ and τ are parameters determined from a fit to the set of generated delays. The deviations of the measurements from the fitted curves are gaussian distributed with a width of 5.1 ps. The parameterization adequately describes the response of all 432 channels in the system.

The TAC response has shown an excellent stability since the commissioning of the electronics. The readout time variations for a single DDG delay,

remain within a 55 ps band over a six month period, even before applying the calibrations.

3.2 Offline Calibration

Even for an ideal TOF detector where all its components are perfectly working, it is still necessary to correct for systematics effects intrinsic to the measurement method. The raw data registered from the $p\bar{p}$ collisions is analyzed 'offline' to characterize and correct such effects.

3.2.1 The timing model

The time t_i at which the discriminator of the channel i is fired, for a track hitting the scintillator at a position z along the length of the bar, is described by:

$$t_i = c_i + t_0 + tof + (L/2 \pm z)/s_j - S_i(Q_i) \quad (3)$$

where Q_i is the registered charge. The constant offset c_i includes, for example, propagation delays in the cables. The t_0 is the time with respect to the nominal bunch crossing. The tof is the particle's time-of-flight. The term $(L/2 \pm z)/s_j$ accounts for the light propagation time inside the bar j , being s_j the speed of light for this bar, (the positive sign is for the west channels and the negative sign for the east channels). The last term describes the time-walk effect introduced by the use of leading edge pulse discriminators.

3.2.2 Time difference analysis

When a single track enters a bar of scintillator, the difference in the times read out on the east and west ends is essentially a linear function of z , the track's entrance point along the bar. A typical distribution of the time difference plotted as a function of z is shown in figure 2, the effective speed of light in the bar comes from the fitted slope.

The width of the residuals for this straight line fit are then a measure of the timing resolution of each PMT, added in quadrature. This resolution averaged over all bars is typically 250 ps or better, since this measures the resolution of two channels added in quadrature, it differs by approximately a factor of two from the resolution expected for a calculation of the mean time from which the time-of-flight is calculated. This indicates that our intrinsic timing resolution is close to the design goals. However, as systematics effects

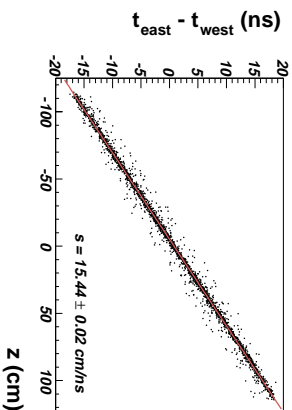


Figure 2: Distribution of the time difference $t_{east} - t_{west}$ vs. the track's entrance point, z .

can cancel in the calculation of the time difference measurement, but would not necessarily cancel in the calculation of time-of-flight, this estimate of the timing resolution only represents the intrinsic capabilities of the detector.

3.2.3 Time-walk correction

The time-walk effect is due to the leading edge pick-off method. Larger pulse heights fire the discriminator at an earlier time than smaller pulse heights. The dependence between the pulse height on the measured time, has been studied using a sample where each track passes through two adjacent bars of scintillator. Depending on the path length in each bar, a range of ADC responses can be obtained in the two channels at the same ends of the bars. Because the z -coordinate of the track's entrance point in each bar is similar, the time difference between the two channels would be nearly identical except for time slewing effects and transit time through the bar. We found an adequate description of the slewing effect for channel i to be equation 4,

$$S_i(Q_i) = \alpha_i \frac{1}{\sqrt{Q_i}} \quad (4)$$

The time difference $T_a - T_b$ between two adjacent channels at the same ends of the bars, corrected by the time of propagation of the light from the entrance point to the bar ends, and by the different particle's time-of-flight between the two bar entrance points, would be identical except for the time slewing effect. Figure 3 shows the dependence between the $T_a - T_b$ time difference with respect to the difference of the time slewing terms $S_a - S_b$. This dependence is essentially linear.

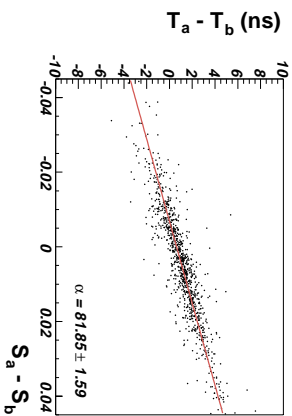


Figure 3: Corrected time difference $T_a - T_b$ as a function of the difference of the time slewing terms in two adjacent channels at the same ends of the bars.

The slewing correction also introduced a linear dependence in the time difference $t_{east} - t_{west}$ versus the entrance point z , resulting in a biased effective speed of light determination. The time-walk corrected speed of light is shown in figure 2. After the correction is applied the width of the speed of light distribution is significantly smaller (the RMS is reduced from $\sim 0.2 \text{ cm/ns}$ to $\sim 0.1 \text{ cm/ns}$) and the low values in the tail have disappeared.

4 TOF resolution

With the described calibrations method we are able to get resolutions of $\sim 130 \text{ ps}$ for tracks passing in front of the photomultipliers. To reach such a close value to the design timing capability, the study has been done on a store by store basis (one store $\approx 0.5 \text{ pb}^{-1}$), using the lepton (J/ψ) trigger.

Thanks to the two-track trigger at CDF [6], that requires two displaced tracks ($120 \text{ } \mu\text{m} < |d_0| < 1 \text{ mm}$) with $p_T > 2 \text{ GeV}/c$, we can use a high statistics sample of $\sim 65 \text{ pb}^{-1}$ to do an independent cross-check of the timing resolution. In particular we analyze the inclusive decay $D^* \rightarrow D^0 \pi^\pm$, $D^0 \rightarrow K\pi$, applying the following selection criteria to get a pure D^* sample:

- One $K\pi$ pair per event
- $1.845 \text{ GeV}/c^2 < M_{K\pi} < 1.875 \text{ GeV}/c^2$
- $M_{K\pi\pi} - M_{K\pi} < 0.1475 \text{ GeV}/c^2$

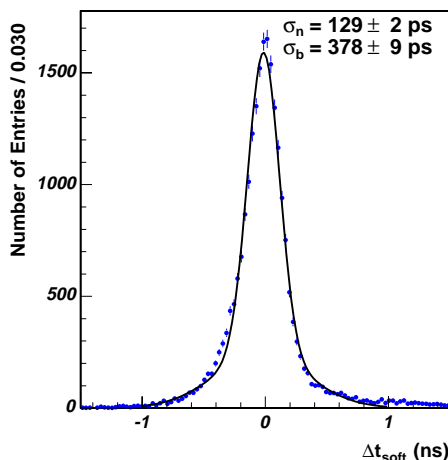


Figure 4: Δt_{soft} distribution. σ_n refers to the narrow gaussian and σ_b refers to the broad gaussian.

- Sideband $\equiv 0.15 \text{ GeV}/c^2 < M_{K\pi\pi} - M_{K\pi} < 0.2 \text{ GeV}/c^2$

After these cuts we get a 97% pure pion sample. The pion that comes from the D^* is commonly called the *soft* pion because its momentum spectrum lies mainly below $1.5 \text{ GeV}/c$, the region where TOF has better particle separation power. We define Δt_{soft} as the difference between the measured and the expected time-of-flight for the *soft* pion assuming it really is a pion,

$$\Delta t_{soft} \equiv t_{of_{measured}}^{soft} - t_{of_{expected}}^{soft} \quad (5)$$

If Δt_{soft} is parameterized with two gaussians (see figure 4) we get a narrow width of $129 \pm 2 \text{ ps}$, in very good agreement with the above results from the calibrations, and a broad width of $378 \pm 9 \text{ ps}$. This second gaussian accounts for the $\sim 33\%$ of the events and it is an understood effect due to some tracks badly skewing the event interaction time (t_0) estimation. An improved track selection for determining the event t_0 has been devised, but not yet implemented in this sample.

5 TOF Trigger

5.1 TOF Trigger Hardware

As one step in achieving a 100 ps timing resolution, the CDF TOF system makes a charge measurement in order to correct discriminator threshold effects. This charge measurement is also a useful quantity for physics triggers as it is proportional to a particle ionization. Pulses are measured by ADMEMs. With suitable reprogramming of the trigger logic, the ADMEMs – which were built for the CDF Calorimetry System – can check if the charge measurement exceeds either of two thresholds. The higher threshold is used for a highly ionizing particle (HIP) trigger, while the lower is used for a minimum ionizing particle (MIP) trigger.

Custom built 9U VME cards – called TOF Trigger Boards (TOTRIBs) – check for a coincidence of exceeded thresholds on both sides of the detector. The MIP coincidences are counted and used for charged particle multiplicity trigger. The MIP coincidence pattern is used for a cosmic ray trigger. The ϕ location of HIP coincidences are compared with extrapolated tracks in the Muon Match-box; any match fires the HIP trigger.

The TOTRIB consists of three coincidence units, which perform the trigger logic, and a VME interface, all implemented on FPGAs. The VME interface controls the board parameters and allows readout by the CDF data acquisition system. The TOF trigger has been running since June 2003.

5.2 Minimum bias QCD

The desired topology is characterized by many tracks in the COT associated to the same event vertex including tracks with transverse momentum as low as feasible (400 MeV/c). This implies that common triggers based on COT or SVX [7] can not be used, being led to a trigger path that includes the TOF detector at Level 1.

In typical Minimum Bias studies, events with charged multiplicity as high as 30 and no significant jet activity are found. Events with no energy clusters of $E_T > 1.1 GeV$ in the calorimeter are more than 50% of the whole sample. Their properties seem to be independent of the center-of-mass-system energy and, in particular, the correlation of the average track p_T versus the charged multiplicity. On the other hand, in the full Minimum Bias sample, the shape of this correlation, not described by any model, is

likely to be strongly connected to the different behavior of the soft and the jet-like components.

In order to analyse the structure of the curve the TOF trigger will be used to collect a sample of events not biased against low p_T tracks. The Level 1 requirement is of 14 MIP hits in TOF and 22 Level 3 COT tracks.

5.3 Search for Magnetic Monopoles

The existence of magnetic monopoles would not just symmetrize Maxwell's Equations of Electrodynamics without breaking any known physical law, but also explain the quantization of the electrical charge in nature according to Dirac's theory. The TOF is a good tool to trigger on events containing magnetic monopoles if they are not too light. The HIP trigger is based on the fact that monopoles heavily ionize material they travel through due to the large coupling to the photons. Monopoles are assumed to be produced from the interaction of a quark/antiquark pair which annihilates into a virtual photon which decays into a monopole/antimonopole pair. This is the Drell-Yan process with the only difference that the photon monopole vertex coupling is different by a factor of $68.5n$ from the photon lepton vertex.

6 Physics with TOF

6.1 B physics

6.1.1 Study of $\Lambda_b \rightarrow \Lambda_c l \nu$, $\Lambda_c \rightarrow p K \pi$

B hadrons consist of a b quark and a cloud of light quarks and gluons. The semileptonic decay of B hadrons is of theoretical interest, since the b ($\sim 4 \text{ GeV}/c^2$) quark is much heavier than the u, d, s ($< 0.15 \text{ GeV}/c^2$) quarks, the semileptonic decay is dominated by the process $b \rightarrow cl\nu$. In the limit of infinite b quark mass, the spectator model predicts that the lifetimes of weakly decaying hadrons containing the same heavy flavor should be identical [8]. A recent study [9] predicts $\tau(\Lambda_b)/\tau(B^0) \approx 0.9 \pm 0.05$ from next-to-leading order corrections to spectator effects in the lifetime ratios of beauty hadrons. Experimentally we expect to reduce the large Run I statistical uncertainty and provide more accurate measurements of the lifetime differences between b -hadrons.

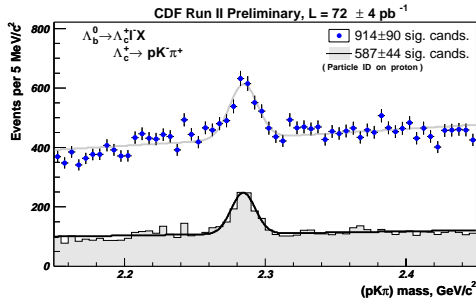


Figure 5: $pK\pi$ invariant mass distribution before (top) and after (bottom) proton particle ID.

Backgrounds to $\Lambda_c \rightarrow pK\pi$ from decays like $D \rightarrow \pi K\pi$ and $D_s \rightarrow KK\pi$ can be greatly reduced by identifying the proton. In figure 5 the invariant mass of $pK\pi$ before and after proton identification is shown. This identification has been made with both dE/dx and TOF, increasing the signal over background ratio (S/B) from 0.18 to 0.53 with a signal efficiency of 64%.

6.2 CHAMP search

Extensions to the Standard Model all imply the existence of as yet undiscovered massive particles that, under a variety of circumstances, can acquire a lifetime that is long compared to the typical time required to traverse the detector. If such a particle is charged, it will present a very distinctive signature in a detector – that of a slowly moving, high transverse momentum charged track. Attendant with the low velocity is a long time-of-flight and an anomalously large ionization energy loss (dE/dx). For a sufficiently massive particle, ionization will in fact dominate the energy loss, even if the particle is strongly interacting [10].

A search for massive long-lived charged particles using $53 pb^{-1}$ of high p_T muon trigger data has been performed at CDF. We expect $2.9 \pm 0.8 \pm 3.1$ events from background and observe seven events, allowing us to set a lower limit of $108 GeV/c^2$ on the mass of an isolated stable scalar top quark.

7 Conclusion

We have described the design of the CDF TOF system which was fully operational and reliably working since October 2001 without any significant problem. Online and offline calibrations have been summarized and resolution results have been shown.

The TOF trigger hardware has been described with some physics that are already using it, such as Minimum Bias QCD and magnetic monopoles search. Other physics analysis that improved thanks to the TOF are Λ_b lifetime, CHAMP search, cosmic rays rejection and still in progress the flavor tagging.

Acknowledgment

The authors would like to thank Marcin Wolter for his contribution in the resolution studies.

References

- [1] R. Blair et al., *The CDF-II Detector Technical Design Report*, FERMILAB-PUB-96/390-E.
- [2] Ch. Paus et al., *Design and Performance Tests of the CDF Time of Flight System*, Nucl. Instrumen. Meth., vol. A461, pp. 579-581, 2001.
- [3] C. Grozis et al., *The Time of Flight Detector at CDF*, Nucl. Phys. Proc. Suppl., vol. 93, pp. 344-347, 2001.
- [4] C. Grozis et al., *A Time of Flight Detector for CDF*, Int. J. Mod. Phys. A16S1C:1119-1121, 2001.
- [5] C. Chen et al., *Front End Electronics for the CDF II Time of Flight System*, Proceedings of the 2001 IEEE Nuclear Science Symposium.
- [6] I. Vila et al., *Performance and First Physics Results of the SVT trigger at CDF II*, FERMILAB-CONF-03/219-E.
- [7] R. Rossin, *The CDF Silicon Vertex Detector for Run II*, Proceedings of the 8th ITCAPP Como 2003 Conference.

- [8] I. I. Bigi, preprint UND-HEP-95-BIG02.
- [9] E. Franco, V. Lubicz, F. Mescia and C. Tarantino, hep-ph/0203089.
- [10] M. Drees and X. Tata, Physics Letter B **252** 695 (1990).